

Fermion–scalar interactions with domain wall fermions

P. Vranas, I. Tziligakis and J. Kogut

Physics Department
University of Illinois
Urbana, IL 61801

April 26, 2024

Abstract

Domain wall fermions are defined on a lattice with an extra direction the size of which controls the chiral properties of the theory. When gauge fields are coupled to domain wall fermions the extra direction is treated as an internal flavor space. Here it is found that this is not the case for scalar fields. Instead, the interaction takes place only along the link that connects the boundaries of the extra direction. This reveals a richness in the way different spin particles are coupled to domain wall fermions. As an application, 4-Fermi models are studied using large N techniques and the results are supported by numerical simulations with $N=2$. It is found that the chiral properties of domain wall fermions in these models are good across a large range of couplings and that a phase with parity-flavor broken symmetry can develop for negative bare masses if the number of sites along the extra direction is finite.

1 Introduction

Domain wall fermions [1] provide an alternative to standard lattice fermions and have already been used to formulate lattice gauge theories (for reviews see [2] and references therein). Here domain wall fermions are used to study lattice theories of fermions and scalars. Such theories can be studied analytically using large N methods and applications of these theories requiring enhanced control over the chiral symmetries may be of interest. For example, such applications may involve 4-Fermi models or models with Higgs fields interacting via Yukawa couplings.

Domain wall fermions (DWF) are defined on the sites of a space-time lattice with one extra direction. The dimension of this lattice will be denoted as $d + 1$. In the method of [3] the boundary conditions along the extra direction are free and as a result light fermion surface states develop on the boundary. The plus chirality components of the Dirac spinor are exponentially localized on one wall while the minus ones are on the other. If the extra direction has L_s sites then the two chiralities overlap only by an amount that is exponentially small in L_s . Therefore, the extra parameter L_s controls the amount by which the regulator breaks the chiral symmetry at any lattice spacing. As a result, and contrary to staggered or Wilson fermions, the chiral and continuum limits are separated. Furthermore, in numerical applications the cost for recovery of the chiral symmetry is only linear in L_s . These properties make DWF an attractive regulator in problems where good control of the chiral symmetries is needed. For example, DWF have been used in studies of the finite temperature QCD phase transition [4, 5, 6, 7, 8].

One would have expected that the formulation of theories with DWF coupled to scalar fields should closely follow that of DWF coupled to gauge fields. However, this is not the case and as a result an interesting difference between the way the scalar and gauge fields are coupled to DWF emerges. The formulation and a discussion of this difference is presented in section 2. Two 4-fermi models, one with a $Z_2 \times Z_2$ and one with an $SU(2) \times SU(2)$ chiral symmetry in three dimensions, are studied in section 3 using large N techniques. In section 4 these models are studied using Hybrid Monte Carlo simulations with $N = 2$. Conclusions are presented in section 5.

Using DWF in 4-Fermi models was also suggested in [9]. For a recent implementation of overlap fermions to the gauged Gross-Neveu model see [10].

2 The fermion–scalar interaction

The free DWF action in the formulation of [3] is:

$$S = - \sum_{x, x', s, s'} \bar{\Psi}(x, s) D(x, s; x', s') \Psi(x', s') \quad (1)$$

with Dirac operator

$$D(x, s; x', s') = \delta(s - s') \mathcal{D}(x, x') + \mathcal{D}^\perp(s, s') \delta(x - x') + E^\perp(s, s'; x) \delta(x - x') \quad (2)$$

where

$$\mathcal{D}(x, x') = \frac{1}{2} \sum_{\mu=1}^d [(1 + \gamma_\mu) \delta(x + \hat{\mu} - x') + (1 - \gamma_\mu) \delta(x' + \hat{\mu} - x)] + (m_0 - d) \delta(x - x') \quad (3)$$

$$\mathcal{D}^\perp(s, s') = \begin{cases} P_R \delta(1 - s') - \delta(s - s') & s = 0 \\ P_R \delta(s + 1 - s') + P_L \delta(s - 1 - s') - \delta(s - s') & 0 < s < L_s - 1 \\ P_L \delta(L_s - 2 - s') - \delta(s - s') & s = L_s - 1 \end{cases} \quad (4)$$

$$E^\perp(s, s') = -m_f [Q_R(s, s') + Q_L(s, s')] \quad (5)$$

$$P_{R,L} = \frac{1 \pm \gamma_5}{2} \quad (6)$$

$$Q_R(s, s') = P_R \delta(L_s - 1 - s) \delta(0 - s'), \quad Q_L(s, s') = P_L \delta(0 - s) \delta(L_s - 1 - s') \quad (7)$$

In the above equations m_0 is a five-dimensional mass representing the “height” of the domain wall. Among other things, the parameter m_0 controls the number of light species [1]. For example, in four dimensions the theory is symmetric around $m_0 = 5$ and for $0 < m_0 < 2$ corresponds to a theory with one light species, for $2 < m_0 < 4$ to a theory with four and for $4 < m_0 < 6$ to a theory with six [11]. The parameter m_f explicitly mixes the two chiralities and as a result it controls the bare fermion mass of the d -dimensional effective theory in a linear fashion. The DWF Dirac operator satisfies the identity [3]:

$$\gamma_5 R D_F \gamma_5 R = D_F^\dagger \quad (8)$$

with R the reflection operator along the fifth direction. As a result, the two species determinant is real and non-negative

$$\det D_F^2 = \det D_F^\dagger D_F \quad (9)$$

From a calculation of the propagator or from the lowest eigenvalue of the fermion matrix the fermion mass for the one flavor free theory is [12]:

$$m_{\text{eff}} = m_0(2 - m_0) [m_f + (1 - m_0)^{L_s}], \quad 0 < m_0 < 2 \quad (10)$$

From the free action one can see that there is more than one way one could couple a gauge field to DWF in a gauge invariant way. The most straightforward choice of introducing a gauge field is to also define it in $d + 1$ dimensions and couple it in the standard gauge invariant way. However, it turns out that this choice does not lead to the correct theory in d dimensions. The correct way to couple the gauge field was arrived at by thinking of the extra dimension as yet another internal flavor space [1, 13]. Then one has to introduce the gauge field only in the d dimensional space and couple it the same way to all fermion “flavors”. Obviously, this also results to a manifestly gauge invariant formulation. In particular, the Dirac operator is as in eq. 2 but with \mathcal{D} defined as:

$$\begin{aligned} \mathcal{D}(x, x') &= \frac{1}{2} \sum_{\mu=1}^d [(1 + \gamma_\mu) U_\mu(x) \delta(x + \hat{\mu} - x') + (1 - \gamma_\mu) U_\mu^\dagger(x') \delta(x' + \hat{\mu} - x)] \\ &+ (m_0 - d) \delta(x - x') \end{aligned} \quad (11)$$

Therefore, although one can think of the extra direction as a new space-time dimension it is more natural to think of it as an internal flavor space. From this point of view, if one wishes to formulate a theory that in d -dimensions would be a theory of a scalar field coupled to a fermion bilinear, one would couple the scalar field to all internal fermion flavors the same way, as was done for the case of a gauge field. However, this choice will not result to the desired theory in d dimensions. To see this consider the simple example of a target theory of fermions coupled to a real valued scalar field σ in d dimensions with continuum action:

$$S = \int \bar{q}\gamma_\mu\partial_\mu q + m\bar{q}q + \sigma\bar{q}q + \beta\sigma^2 \quad (12)$$

If $m = 0$ this model has a $Z_2 \times Z_2$ chiral symmetry. It is clear that a large N or mean field analysis of this model will indicate that the propagator mass would be $m_+ < \sigma >$ where $< \sigma >$ is the vacuum expectation value of the σ field. Clearly a lattice formulation of this model using DWF should at least reproduce this simple result. However, if the σ field is coupled to all fermion degrees of freedom the same way, as is the mass m_0 , i.e. $\bar{\Psi}(x, s)\sigma(x)\Psi(x, s)$, a similar analysis will result to a propagator mass as in eq. 10, but with m_0 replaced by $m_0 + < \sigma >$. This is obviously the wrong result. Even if one was to accept this exponential behavior by redefining the σ field this theory would have the peculiar property of changing the number of light species depending on the value of σ . Clearly, in order to get the correct result one has to couple the σ field in the same fashion as the m_f mass and not as the $d + 1$ mass m_0 . Then the Dirac operator is as in eq. 2 but with E^\perp :

$$E^\perp(s, s'; x) = -[m_f + \sigma(x)] [Q_R(s, s') + Q_L(s, s')] \quad (13)$$

In the resulting action the σ field couples with the fermion fields only across the boundary links of the $d + 1$ dimension. That this is the correct action can be seen by observing that the interaction term in the action can be rewritten as:

$$\bar{\Psi}(x, L_s - 1)\sigma(x)P_R\Psi(x, 0) + \bar{\Psi}(x, 0)\sigma(x)P_L\Psi(x, L_s - 1) = \bar{q}(x)\sigma(x)q(x) \quad (14)$$

with:

$$\begin{aligned} q(x) &= P_R\Psi(x, 0) + P_L\Psi(x, L_s - 1) \\ \bar{q}(x) &= \bar{\Psi}(x, L_s - 1)P_R + \bar{\Psi}(x, 0)P_L \end{aligned} \quad (15)$$

The fields \bar{q}, q correspond to the light d -dimensional fields [3]. Since these are the only propagating fields in d dimensions and since, in terms of these fields the correct global symmetry is in place, the above action should describe the desired target theory.

Another way to see that this is the correct action is to consider adding such an interaction to Neuberger fermions [14]. In that formulation the fermion fields are standard d dimensional fields and the interaction can be added unambiguously. Then if the discrete finite flavor version of that formulation is used one can directly recover the DWF action. Since the σ field is added as a mass term, one can see by simple inspection that the above action is recovered. Furthermore, the connection can also be made exact by using the results of [15] where the d -dimensional action arrived at by integrating all heavy fermion degrees of freedom is expressed solely in terms of the \bar{q}, q fields.

It should also be noted that scalar fields were used in a different context [1, 16] in an attempt to formulate chiral gauge theories using DWF. There, in order to maintain gauge invariance, the scalar fields were defined on a “slice” in the extra direction.

With the interaction defined as in eq. 13 the transfer matrix of the model along the $d + 1$ direction [13, 3] is independent of the σ field and is therefore the free field transfer matrix. The σ field is defined only on the boundary and therefore only affects the boundary operator \mathcal{O} of [3]. In the case of a gauge theory the extra fermion degrees of freedom are heavy but numerous as the $L_s \rightarrow \infty$ limit is taken. For this reason it was shown that they need to be subtracted and the way to do that for each gauge field background is to divide out a bulk factor [13] of the form $f(U)^{L_s}$ where $f(U)$ is some function of the gauge field U determined by the transfer matrix (in the formulation of [3] $f(U) = \lambda_{\max} \det B$). Here the same bulk factor is present but unlike the gauge theory it does not depend on the background field. Therefore it can be factored out from the σ path integral and as a result it becomes an irrelevant factor that will cancel out with the same factor coming by dividing by the partition function whenever an expectation value is calculated. Therefore, unlike the gauge theory, it is unnecessary to explicitly subtract it out.

The extension to more general interaction terms is straightforward. The interaction is written in terms of the \bar{q}, q fields and using eq. 15 is transcribed for the $\bar{\Psi}, \Psi$ fields. For example, a target theory with $SU(2) \times SU(2)$ chiral symmetry has Dirac operator as in eq. 2 but with E^\perp :

$$E^\perp(s, s'; x) = -[m_f + \sigma(x) + i\gamma_5 \boldsymbol{\pi}(x) \cdot \boldsymbol{\tau}] [Q_R(s, s') + Q_L(s, s')] \quad (16)$$

where $\boldsymbol{\pi}(x)$ is the pion field and $\boldsymbol{\tau}$ are the Pauli matrices.

The above results, although contrary to naive expectations, are straightforward. However, the following observations can be made:

- 1) For the case of scalar fields it is not natural to interpret the extra DWF direction as an internal flavor space since the interaction takes place only at the boundary of the extra direction.
- 2) One could have thought that the introduction of an extra dimension would have lent some freedom in the definition of the DWF interaction with the scalar and gauge fields. However, this appears not to be the case. The DWF formalism and symmetry requirements seem to have naturally forced the interaction terms to be of this specific form.
- 3) A picture with some richness seems to develop with different spin fields coupled to domain wall fermions in different ways.

3 Large N analysis

The analysis in this section closely follows the analysis in [17] of the same model using Wilson fermions. Also see [18, 19, 20, 21] for studies of 4-Fermi models with staggered fermions.

Consider a 4-Fermi model in the continuum with $SU(2) \times SU(2)$ chiral symmetry and Lagrangian:

$$\mathcal{L} = \bar{q}(i\partial - m)q + \frac{G_1}{2} [(\bar{q}q)^2 + (\bar{q}i\gamma_5\boldsymbol{\tau}q)^2]. \quad (17)$$

In the above expression all indices have been suppressed. The fermionic field q is a flavor $SU(2)$ doublet and a color $SU(N)$ N -column vector. The Lagrangian is diagonal in “color”, in contrast with the full QCD Lagrangian which is diagonal in flavor. $\boldsymbol{\tau} = \{\tau_1, \tau_2, \tau_3\}$ are the three isospin Pauli matrices, $\not{\partial} = \gamma^\mu \partial_\mu$, and m is the bare quark mass (if $m \neq 0$ the chiral symmetry is explicitly broken). As is well known, a Lagrangian density that is quadratic in the fermionic fields can be obtained by introducing a scalar auxiliary field σ and three pseudoscalar auxiliary fields $\boldsymbol{\pi} = \{\pi_1, \pi_2, \pi_3\}$ coupled to the fermion bilinear:

$$\begin{aligned}\mathcal{L} &= \bar{q}Dq - n_f\beta_1(\sigma^2 + \boldsymbol{\pi}^2) \\ D &= i\not{\partial} - m - \sigma - i\gamma_5\boldsymbol{\tau} \cdot \boldsymbol{\pi} \quad .\end{aligned}\tag{18}$$

Here n_f is the number of flavors and $\beta_1 = \frac{1}{2n_f G_1}$. Transcribing this to a Euclidian lattice, using DWF with fermion-scalar interaction as described in section 2 and an even number of “colors” N one obtains:

$$\begin{aligned}Z &= \int [d\Psi d\bar{\Psi} d\sigma d\boldsymbol{\pi}] e^{-S} \\ S &= \sum_{i=1}^{N/2} \left\{ \bar{\Psi}^i D \Psi^i + \bar{\Psi}^{i+N/2} D^\dagger \Psi^{i+N/2} \right\} + n_f \beta_1 (\sigma^2 + \boldsymbol{\pi}^2)\end{aligned}\tag{19}$$

where D is defined in eq. 2 with E^\perp as in eq. 16 and use of the property in eq. 9 has been made.

Following the standard large N analysis, the saddle point equations (SPE) are calculated by assuming uniform saddle fields and small fluctuations of the form:

$$\sigma(x) = \sigma_s + \frac{\delta\sigma(x)}{\sqrt{N}}, \quad \boldsymbol{\pi}(x) = \boldsymbol{\pi}_s + \frac{\delta\boldsymbol{\pi}(x)}{\sqrt{N}}\tag{20}$$

The saddle point equations are:

$$\frac{1}{V} \text{ReTr}[D_s^{-1}(Q_R + Q_L)] + 2n_f \bar{\beta}_1 \sigma_s = 0\tag{21}$$

$$\frac{1}{V} \text{ReTr}[D_s^{-1}(Q_R + Q_L) i\gamma_5 \boldsymbol{\tau}] + 2n_f \bar{\beta}_1 \boldsymbol{\pi}_s = 0\tag{22}$$

or in terms of the \bar{q}, q fields of eq. 15:

$$\frac{1}{V} \text{Re} \langle \bar{q}q \rangle_s + 2n_f \bar{\beta}_1 \sigma_s = 0\tag{23}$$

$$\frac{1}{V} \text{Re} \langle \bar{q} i\gamma_5 \boldsymbol{\tau} q \rangle + 2n_f \bar{\beta}_1 \boldsymbol{\pi}_s = 0\tag{24}$$

where

$$\bar{\beta}_1 = \frac{\beta_1}{N} = \frac{1}{2n_f N G_1}\tag{25}$$

The $L_s = \infty$ and the finite L_s cases need to be studied separately since each case has a different symmetry group.

I. The $L_s = \infty$ case.

If $m_f = 0$ then the DWF Dirac operator has exact chiral symmetry. If there is spontaneous symmetry breaking one is therefore free to choose the direction of breaking at will. The standard choice is $\sigma_s \neq 0$ and $\boldsymbol{\pi}_s = 0$. For this choice the second SPE eq. 22 is trivially satisfied since the non-trivial flavor part of D_s^{-1} is proportional to $\boldsymbol{\tau}\boldsymbol{\pi}_s$. This case is identical to the case of a simpler model without $\boldsymbol{\pi}$ fields and $n_f = 1$. Such a theory has $Z_2 \times Z_2$ chiral symmetry. Therefore, the following analysis can be trivially extended for the $Z_2 \times Z_2$ model.

Using the free propagator results of [12] after some algebra the first SPE eq. 21 for $L_s = \infty$ results in:

$$\sigma_s \bar{\beta}_1 - \frac{2(\sigma_s + m_f)}{V} \sum_p \frac{z(p)^2}{\bar{p}^2 + (\sigma_s + m_f)^2 z(p)^2} = 0 \quad (26)$$

where

$$\bar{p}^2 = \sum_{\mu=1}^d \sin(p_\mu)^2 \quad (27)$$

$$z(p) = 1 - be^{-a} \quad (28)$$

$$b = 1 - m_0 + \sum_{\mu=1}^d (1 - \cos(p_\mu)) \quad (29)$$

$$\cosh a = \frac{1 + b^2 + \bar{p}^2}{2b}, \quad 0 \leq a \quad (30)$$

The factor $z(p)$ plays the role of “selecting” Brillouin zones. For a given range of m_0 the factor $z(p)$ is nonzero at the origins of only certain Brillouin zones. To see this observe that at the origin of any Brillouin zone $\bar{p} \approx 0$ and therefore eq. 30 has solution $\exp(-a) = b$ if $|b| < 1$ and $\exp(-a) = 1/b$ if $|b| > 1$. Therefore, from eq. 28, one can see that $z(p) = 1 - b^2$ if $|b| < 1$ and $z(p) = 0$ if $|b| > 1$. For example, if $0 < m_0 < 2$ then $z(p)$ is non zero only in the zone with momentum components around zero. The condition for nonzero $z(p)$ at the origins of a Brillouin zone:

$$|b| < 1 \Leftrightarrow m_0 - 2 < \sum_{\mu=1}^d (1 - \cos(p_\mu)) < m_0 \quad (31)$$

is the same as the condition for the existence of normalizable states [1]. For zero momentum $z(\mathbf{p} = 0) = m_0(2 - m_0)$.

One can see that eq. 26 for $m_f = 0$ can have two solutions: one with $\sigma_s = 0$ corresponding to a chirally symmetric phase, and one with $\sigma_s \neq 0$ corresponding to a phase with spontaneously broken chiral symmetry. The critical value of $\bar{\beta}_1$ is obtained from eq. 26 in the limit $\sigma_s \rightarrow 0$ and is given by:

$$\bar{\beta}_{1c} = \frac{2}{V} \sum_p \frac{z(p)^2}{\bar{p}^2} \quad (32)$$

It is interesting to notice the rather strong dependence of $\bar{\beta}_{1c}$ on m_0 . Similarly strong dependence of the critical coupling on m_0 was found for the QCD finite temperature phase

transition [4]. As an example, $\bar{\beta}_{1c}$ is plotted versus m_0 for a 6^3 lattice with antiperiodic boundary conditions along the time direction in figure 1. In the next section such lattices will be used to compare the large N expressions with numerical simulations. A similar graph can be obtained for a four-dimensional lattice but it extends from $m_0 = 0$ to $m_0 = 10$ and is symmetric around $m_0 = 5$.

II. The finite L_s case.

When L_s is finite the DWF Dirac operator breaks chiral symmetry explicitly even for $m_f = 0$. Therefore $\sigma_s \neq 0$ and the remaining symmetry is the $SU(2)$ flavor symmetry. This symmetry can break spontaneously resulting to a nonzero π_s . If this happens then from eq. 24 one can see that $\langle \bar{q}i\gamma_5\tau q \rangle \neq 0$ and the parity as well as flavor symmetries are broken. This is the Aoki phase [22]. This phase has also been observed for this model with Wilson fermions [23, 24]. The existence of this phase for DWF was also suggested in [25] and it may be present in QCD with DWF [26].

First consider the phase with $\pi_s = 0$. Again the second SPE eq. 22 is trivially satisfied and the following analysis is also valid for the $Z_2 \times Z_2$ model at finite L_s . The first SPE eq. 22 is:

$$\begin{aligned} \sigma_s \bar{\beta}_1 - \frac{2}{V} \sum_p \{ & (m_f + \sigma_s)(A_0 + A_2) + bA_m \\ & + e^{-a(L_s-1)} [(m_f + \sigma_s)A_m + b(B + A_1 + A_2)] \\ & + e^{-2a(L_s-1)} [(m_f + \sigma_s)A_1 + bA_m] \} = 0 \end{aligned} \quad (33)$$

where A_0, A_1, A_2, A_m are functions of the momentum, $m_f + \sigma_s$ and e^{-aL_s} and are the same as in [12] but with m_f replaced by $m_f + \sigma_s$. This equation can be used to calculate σ_s as a function of the other parameters of the theory.

It is interesting to see how chiral symmetry is restored as L_s increases. As can be seen from eq. 30 the decay coefficient a is independent of $\bar{\beta}_1$ and it only depends on m_0 and the momenta. In figure 2 the minimum and the maximum value of $Re(a)$ (if $b < 0$ a has imaginary part $\pm i\pi$) obtained for different momenta is plotted as a function of m_0 in the range $0 < m_0 < 2$. The ‘‘spikes’’ of the maximum value are the singularities that occur when $b = 0$. As can be deduced from eq. 30 the peak of the minimum decay occurs at $m_0 = 2 - \sqrt{2} = 0.586$ and is $-\ln(2 - \sqrt{2}) = 0.535$. The decay rates between the minimum and the maximum values have no gaps. As L_s increases eventually the only chiral symmetry violations that remain will be controlled by the minimum decay rate unless the observable is dominated solely by terms with decay rate close to the maximum. Since the minimum decay rate is approximately constant across the full range of m_0 there is no valuable option of tuning m_0 in order to achieve better characteristics except perhaps around $m_0 = 0.586$. As an example, σ_s versus L_s is plotted in figure 3 for $m_f = 0$ and various m_0 at $\bar{\beta}_1 = 0.3$ which is above the transition for all the m_0 values. The slopes obtained from the larger L_s points are slightly faster than the minimum decay rates of figure 2 and the largest slope is for $m_0 = 0.6$.

Next consider the phase with $\pi_s \neq 0$. The first SPE is as in the $\pi = 0$ case eq. 33. However, since the non-trivial flavor part of D_s^{-1} is proportional to $\tau\pi_s$ one can now eliminate π_s from the second SPE and obtain a second non trivial equation. These two equations can be used to determine σ_s and π_s . The full form of these equations is

complicated and not particularly illuminating. However, if only the leading order in m_f and e^{-aL_s} is kept these equations can be written in the form:

$$\bar{\beta}_1 = \frac{2}{V} \sum_p \left[\frac{z^2}{D} \right] + O(1) \quad (34)$$

$$m_f = -\frac{\sum_p \left[e^{-aL_s} \left(\frac{\bar{p}^2 + z^2}{D} \right) \right]}{\sum_p \left[\frac{z^2}{D} \right]} + O(2) \quad (35)$$

$$D = \bar{p}^2 \left(1 + [m_f + \sigma_s] e^{-aL_s} \right)^2 + z^2 \left([m_f + \sigma_s] + e^{-aL_s} \right)^2 + |\boldsymbol{\pi}_s|^2 \left(z^2 + \bar{p}^2 e^{-2aL_s} \right) \quad (36)$$

If L_s is an even number or if m_0 is such that $0 \leq b(p)$ (and therefore $0 \leq e^{-a(p)}$) for all momenta then e^{-aL_s} is positive and m_f must be negative in order to have a phase with $\boldsymbol{\pi}_s \neq 0$. The phase boundary $m_{f_c}(\bar{\beta}_1)$ can be obtained from the above equations by setting $\boldsymbol{\pi}_s \rightarrow 0$ and eliminating $x = m_f + \sigma_s$. From these equations it can be deduced that $|m_{f_c}|$ decreases exponentially with L_s . Furthermore, for a given $\bar{\beta}_{1c}$ the width of the $\boldsymbol{\pi}_s \neq 0$ region also decreases exponentially with L_s . In figure 4 the phase boundary of the $\boldsymbol{\pi}_s \neq 0$ phase is given for a 6^3 lattice with antiperiodic boundary conditions along the time direction, $m_0 = 1$ and for various L_s values. From bottom to top the L_s values are 2, 3, 4, and 5. This has been calculated using the full form of the SPE and not just the truncated form eq. 34 and 35. However, the two are nearly the same for $2 < L_s$. Also different values of m_0 produce similar results. As can be seen from figure 4 when L_s is increased the phase boundary moves to smaller $|m_f|$ with decreasing width. In figure 5 for fixed $\bar{\beta}_1 = 0.05$ the origin of the phase boundary $-m_{f_c}$ and width δm_{f_c} are plotted versus L_s for $m_0 = 1.0$ and a 6^3 lattice with antiperiodic boundary conditions along the time direction.

The effective fermion mass m_q is identified from the zero of eq. 36 for momenta $\mathbf{p} \approx 0$ and is:

$$m_q = z(\mathbf{p} = 0)[m_f + \sigma_s + (1 - m_0)^{L_s}] \quad (37)$$

The continuum limit is reached at $m_q = 0$ and the lattice spacing is set to $\alpha \sim m_q$. This point corresponds to the largest $\bar{\beta}_{1c}$ value of the phase boundary curves in figure 4 (m_q is positive on the upper part of the phase boundary and negative on the lower one). The width of the Aoki phase close to $m_q = 0$ can be obtained from eq. 35. To lowest order in m_q is: $\delta m_f = m_q \frac{\partial m_f}{\partial m_q} \Big|_{m_q=0}$. The derivative is not zero at $m_q = 0$ and therefore $\delta m_f \sim m_q \sim \alpha$. For an analysis concerning the width of the Aoki phase in QCD with Wilson fermions see [27]. The above features are not particular to three dimensions and similar results have been obtained for four-dimensional lattices.

Finally, it is interesting to observe that if m_0 is such that $b(p) \leq 0$ for some momenta and L_s is odd then the $\boldsymbol{\pi}_s \neq 0$ phase can occur even for positive m_f . If the $\boldsymbol{\pi}_s \neq 0$ phase needs to be avoided for any m_0 then one should set $0 \leq m_f$ and L_s to an even number (on the other hand, if $m_0 \leq 1$ then $0 \leq b(p)$ for any momenta and any value of L_s can be used).

4 Hybrid Monte Carlo simulations

In this section standard Hybrid Monte Carlo (HMC) simulations are performed for $N = 2$. These simulations support the large N results of the previous section. For all simulations

the trajectory length is set to $\tau = 1$ and the step size to $\delta\tau = 0.1$. The acceptance rate is $\approx 90\%$ and the conjugate gradient inverter iterations are $\approx 50 - 100$. Typically 100 – 200 thermalization sweeps were followed by 300 – 400 sweeps with measurements. The lattice size for all simulations is 6^3 with antiperiodic boundary conditions along the time direction. All simulations were done on workstations.

The $Z_2 \times Z_2$ model with action as in eq. 1 and interaction term as in eq. 13 was simulated first. The initial configuration for all simulations was a uniform configuration with $\sigma = 1$. In figure 6, $\langle \sigma \rangle$ is plotted as a function of $\bar{\beta}_1$ for $m_f = 0.02$, $L_s = 12$, $m_0 = 0.4$ (diamonds), $m_0 = 1.0$ (squares) and $m_0 = 1.6$ (crosses). The solid lines are the large N predictions for the same parameters and the dotted lines are the large N predictions for $m_f = 0$ and $L_s = \infty$. The agreement with the large N predictions is good away from the critical region where the approximation of a uniform saddle is good.

The decay and decay rate of $\langle \sigma \rangle$ as a function of L_s for $m_f = 0.02$ is shown in figure 7. In figure 7a $m_0 = 1.0$ and $\bar{\beta}_1 = 0.05$ (diamonds), $\bar{\beta}_1 = 0.1$ (squares) and $\bar{\beta}_1 = 0.25$ (crosses). In figure 7c $\bar{\beta}_1 = 0.05$ and $m_0 = 0.6$ (diamonds), $m_0 = 0.8$ (squares), $m_0 = 1.0$ (crosses), and $m_0 = 1.1$ (circles). The solid lines in figures 7a and 7c are fits to $c_0 + c_1 e^{-c_2 L_s}$ and the dotted lines are the large N predictions. The decay rates c_2 from the fits in figures 7a and 7c are shown in figures 7b and 7d respectively. The solid lines in these figures are the large N predicted minimum and maximum decay rates. As can be seen, the agreement with the large N predictions is good and the decay rates are fairly independent of $\bar{\beta}_1$ and m_0 and close to the minimum predicted value. This is in contrast to gauge theories where the dependence of the decay rates on the gauge coupling is significant [12, 4].

Finally the $SU(2) \times SU(2)$ model with action as in eq. 1 and interaction term as in eq. 16 was simulated in an effort to investigate the presence of the parity-flavor broken phase. The lattice Lagrangian has exact $SU(2)$ flavor symmetry and as a result when this symmetry is spontaneously broken there will be two exactly massless Goldstone pions. In that case the Conjugate Gradient inverter would not converge. Furthermore, in the small lattices considered here spontaneous breaking can not really take place and the $\boldsymbol{\pi}$ field would always average to zero for sufficiently large statistics. In [22, 28, 29] these problems were treated by adding a small external field \boldsymbol{h} that breaks the $SU(2)$ flavor symmetry and therefore not only gives mass to the two pions but also provides a “preferred” orientation for the $\boldsymbol{\pi}$ field. Such an external field is used here by adding a term that is exactly the same as the $\boldsymbol{\pi}$ term in eq. 16 but with $\boldsymbol{\pi}$ replaced by \boldsymbol{h} . The initial configuration for all simulations was a uniform configuration with $(\sigma, \pi_1, \pi_2, \pi_3) = (1, 0, 0, 1)$. In figure 8 the average value of π_3 is plotted versus m_f for a 6^3 lattice with antiperiodic boundary conditions along the time direction, $\boldsymbol{h} = (0, 0, 0.1)$, $\bar{\beta}_1 = 0.05$, $L_s = 2$ and $m_0 = 1.0$. The “outer” solid line is the large N prediction for $\boldsymbol{h} = (0, 0, 0.1)$ and the “inner” one for $\boldsymbol{h} = (0, 0, 0)$. The diamonds are the results of the numerical simulations. As can be seen they are in fairly good agreement with the large N results supporting the presence of this phase. A finite volume analysis together with an analysis involving decreasing values of \boldsymbol{h} as in [29] is still needed in order to unequivocally establish the presence of the parity-flavor broken phase for $N = 2$, but this is not in the scope of this paper.

5 Conclusions

The interaction of domain wall fermions with scalar fields was formulated. It was found that contrary to naive expectations this interaction takes place only at the boundary of the extra direction. This is in contrast to the interaction of domain wall fermions with gauge fields which is the same along the extra direction. This seems to indicate a picture with some richness where different spin fields couple to domain wall fermions in different ways.

Large N techniques were used to study two 4-Fermi models, one with $Z_2 \times Z_2$ and one with $SU(2) \times SU(2)$ chiral symmetry. It was found that at the limit of infinite extra direction the chiral symmetry breaks spontaneously in the standard fashion. However, if the size of the extra direction is finite the $SU(2) \times SU(2)$ chiral symmetry is explicitly broken by the regulator down to flavor $SU(2)$. It was found that this remaining flavor symmetry can break spontaneously if the bare quark mass is negative resulting to a parity-flavor broken phase of the Aoki type. Hybrid Monte Carlo simulations were performed for those models with $N = 2$ on 6^3 lattices with antiperiodic boundary conditions along the extra direction. The results were found to support the large N predictions.

Acknowledgments

We thank G. Fleming for useful comments. This research was supported in part by NSF under grant # NSF-PHY96-05199.

References

- [1] D.B. Kaplan, Phys. Lett. **B288** (1992) 342; Nucl. Phys. **B30** (Proc. Suppl.) (1993) 597.
- [2] R. Narayanan, Nucl. Phys. **B34** (Proc. Suppl.) (1994) 95; M. Creutz, Nucl. Phys. **B42** (Proc. Suppl.) (1995) 56; Y. Shamir, Nucl. Phys. **B47** (Proc. Suppl.) (1996) 212; T. Blum, to appear in the Lattice 98 conference proceedings, hep-lat/9810017.
- [3] V. Furman, Y. Shamir, Nucl. Phys. **B439** (1995) 54.
- [4] P. Chen, N. Christ, G. Fleming, A. Kaehler, C. Malureanu, R. Mawhinney, G. Siegert, C. Sui, P. Vranas, and Y. Zhestkov, contribution to Lattice 98, hep-lat/9809159.
- [5] P. Chen, N. Christ, G. Fleming, A. Kaehler, C. Malureanu, R. Mawhinney, G. Siegert, C. Sui, P. Vranas, and Y. Zhestkov, contribution to Lattice 98, hep-lat/9811013.
- [6] P. Chen, N. Christ, G. Fleming, A. Kaehler, C. Malureanu, R. Mawhinney, G. Siegert, C. Sui, P. Vranas, and Y. Zhestkov, contribution to Lattice 98, talk by A. Kaehler.
- [7] P. Chen, N. Christ, G. Fleming, A. Kaehler, C. Malureanu, R. Mawhinney, G. Siegert, C. Sui, P. Vranas, and Y. Zhestkov, contribution to ICHEP 98, hep-lat/9812011.
- [8] P. Vranas, contribution to DPF 99, hep-lat/9903024.

- [9] K.M. Bitar, personal communication with P. Vranas.
- [10] I. Ichinose and K. Nagao, hep-lat/9905001.
- [11] P. Chen, N. Christ, G. Fleming, A. Kaehler, C. Malureanu, R. Mawhinney, G. Siegert, C. Sui, P. Vranas, and Y. Zhestkov, contribution to Lattice 98, hep-lat/9811026.
- [12] P.M. Vranas, Lattice 96, Nucl. Phys. **B53** (Proc. Suppl.) (1997) 278; Phys. Rev. **D57** (1998) 1415.
- [13] R. Narayanan, H. Neuberger, Phys. Lett. **B302** (1993) 62; Phys. Rev. Lett. **71** (1993) 3251; Nucl. Phys. **B412** (1994) 574; Nucl. Phys. **B443** (1995) 305.
- [14] H. Neuberger, Phys. Rev. **D57** (1998) 5417; Phys. Lett. **B417** 141 (1998); Phys. Rev. Lett. **81** (1998) 4060; hep-lat/9901003; U.M. Heller, R. Edwards and R. Narayanan hep-lat/9807017; hep-lat/9811030; C. Lieu, hep-lat/9811008.
- [15] Y. Kikukawa, T. Noguchi, hep-lat/9902022.
- [16] M. Golterman, K. Jansen, D. Petcher and J. Vink, Phys. Rev. **D49** (1994) 1606.
- [17] K.M. Bitar and P.M. Vranas, Phys.Lett. **B327** (1994) 101; Nucl. Phys. **B34** (Proc. Suppl.) (1994) 661; Phys. Rev. **D50** (1994) 3406.
- [18] S. Hands, A. Kocic, J.B. Kogut, Annals Phys. **224** (1993) 29; Nucl. Phys. **B390** (1993) 355.
- [19] A. Kocic, J.B. Kogut, Phys. Rev. Lett. **74** (1995) 3109; Nucl. Phys. **B455** (1995) 229.
- [20] S. Kim, J.B. Kogut, M.P. Lombardo Nucl. Phys. **B53** (Proc.Suppl) (1997) 709.
- [21] A. Ali Khan, M. Gockeler, R. Horsley, P.E.L. Rakow, G. Schierholz, H. Stuben, Nucl. Phys. **B34** (Proc.Suppl.) (1994) 655; Int. J. Mod. Phys. **C5** (1994) 351.
- [22] S. Aoki, Phys. Rev. **D30** (1984) 2653.
- [23] S. Aoki, S. Boettcher and A. Gocksch, Phys. Lett. **B331** (1994) 157.
- [24] K.M. Bitar and P.M. Vranas, Nucl. Phys. **B42** (Proc. Suppl.) (1995) 746.
- [25] R. Narayanan, personal communication with P. Vranas.
- [26] RIKEN-BNL-Columbia lattice group, in progress.
- [27] S. Sharpe and R. Singleton, Phys. Rev. **D58** (1998) 074501.
- [28] S. Aoki and A. Gocksch, Phys. Rev. **D45** (1992) 3845.
- [29] K.M. Bitar, Nucl. Phys. **B63** Proc. Suppl. (1998) 829; Phys. Rev. **D56** (1997) 2736.

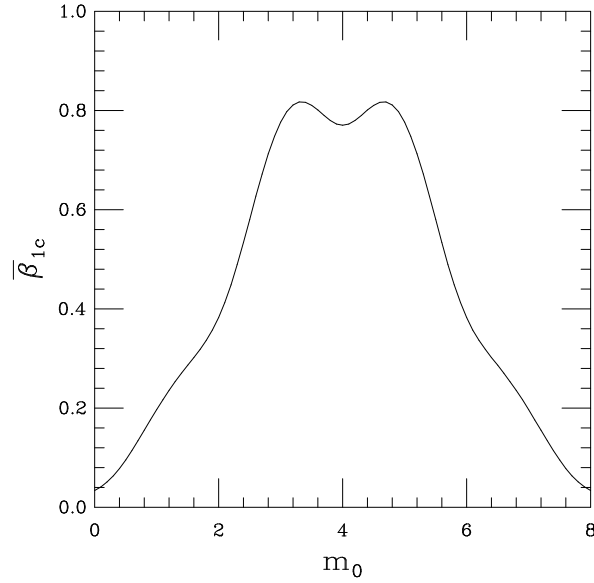


Figure 1. The large N critical value $\bar{\beta}_{1c}$ versus m_0 for a 6^3 lattice with antiperiodic boundary conditions along the time direction.

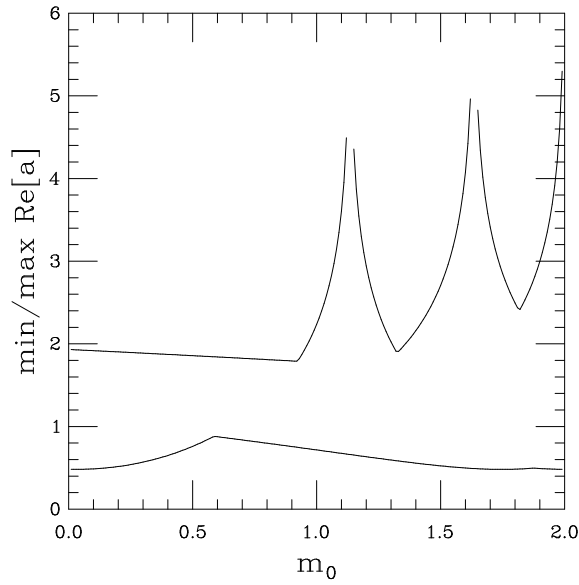


Figure 2. The real part of the maximum and minimum large N decay rates as a function of m_0 for a 6^3 lattice with antiperiodic boundary conditions along the time direction.

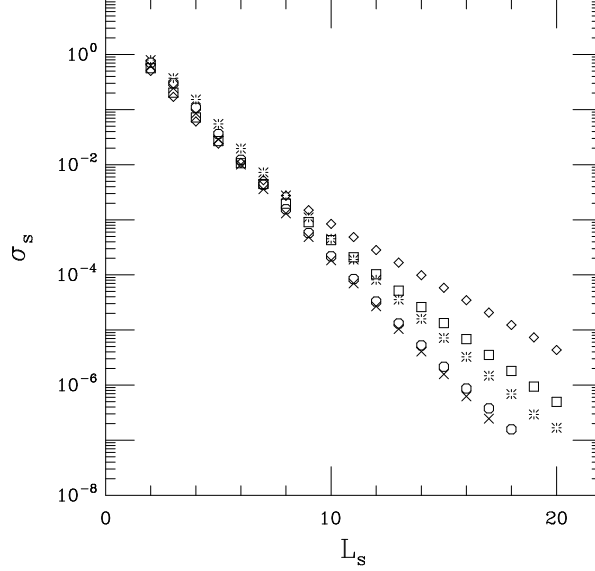


Figure 3. The large N σ_s as a function of L_s for a 6^3 lattice with antiperiodic boundary conditions along the time direction, $m_f = 0$ and various m_0 at $\bar{\beta}_1 = 0.3$ above the transition. The diamonds, squares, crosses, circles, and stars correspond to $m_0 = 0.2, 0.4, 0.6, 0.8, 1.0$.

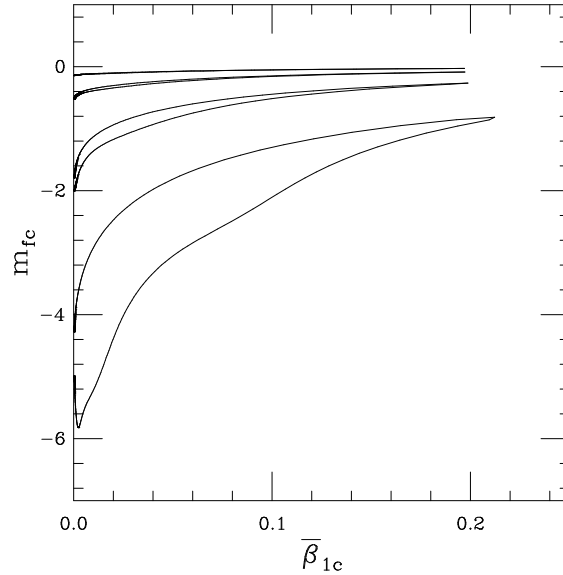


Figure 4. The large N phase boundary of the parity-flavor broken phase of the $SU(2) \times SU(2)$ model on a 6^3 lattice with antiperiodic boundary conditions along the time direction with $m_0 = 1$ and for various L_s values. From bottom to top the L_s values are 2, 3, 4, and 5. The parity-flavor symmetry is broken inside the oval-looking regions.

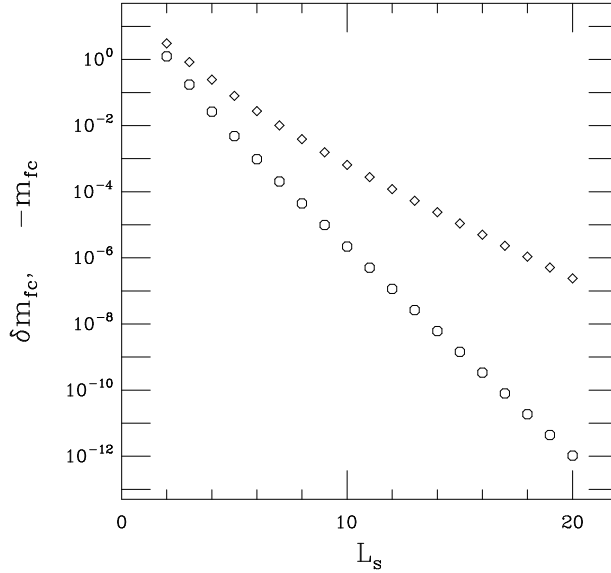


Figure 5. For fixed $\bar{\beta}_1 = 0.05$ the origin $-m_{fc}$ (diamonds) and width δm_{fc} (circles) of the large N parity-flavor broken phase of the $SU(2) \times SU(2)$ model is plotted versus L_s for $m_0 = 1$ and for a 6^3 lattice with antiperiodic boundary conditions along the time direction.

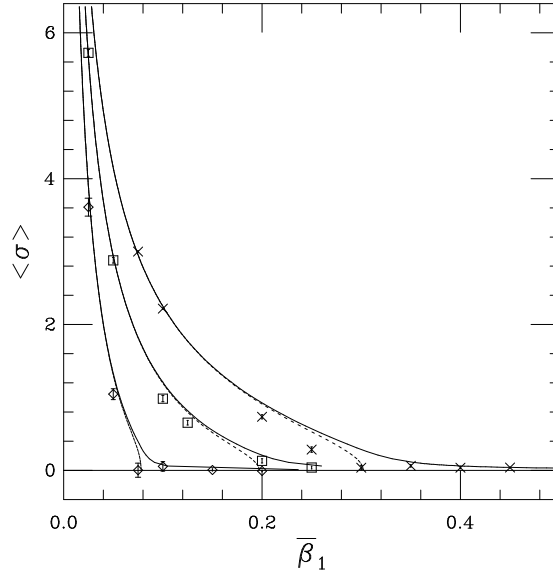


Figure 6. $\langle \sigma \rangle$ as a function of $\bar{\beta}_1$ for the $Z_2 \times Z_2$ model on a 6^3 lattice with antiperiodic boundary conditions along the time direction, $m_f = 0.02$, $L_s = 12$, $m_0 = 0.4$ (diamonds), $m_0 = 1.0$ (squares) and $m_0 = 1.6$ (crosses). The solid lines are the large N predictions for the same parameters and the dotted lines are the large N predictions for $m_f = 0$ and $L_s = \infty$.

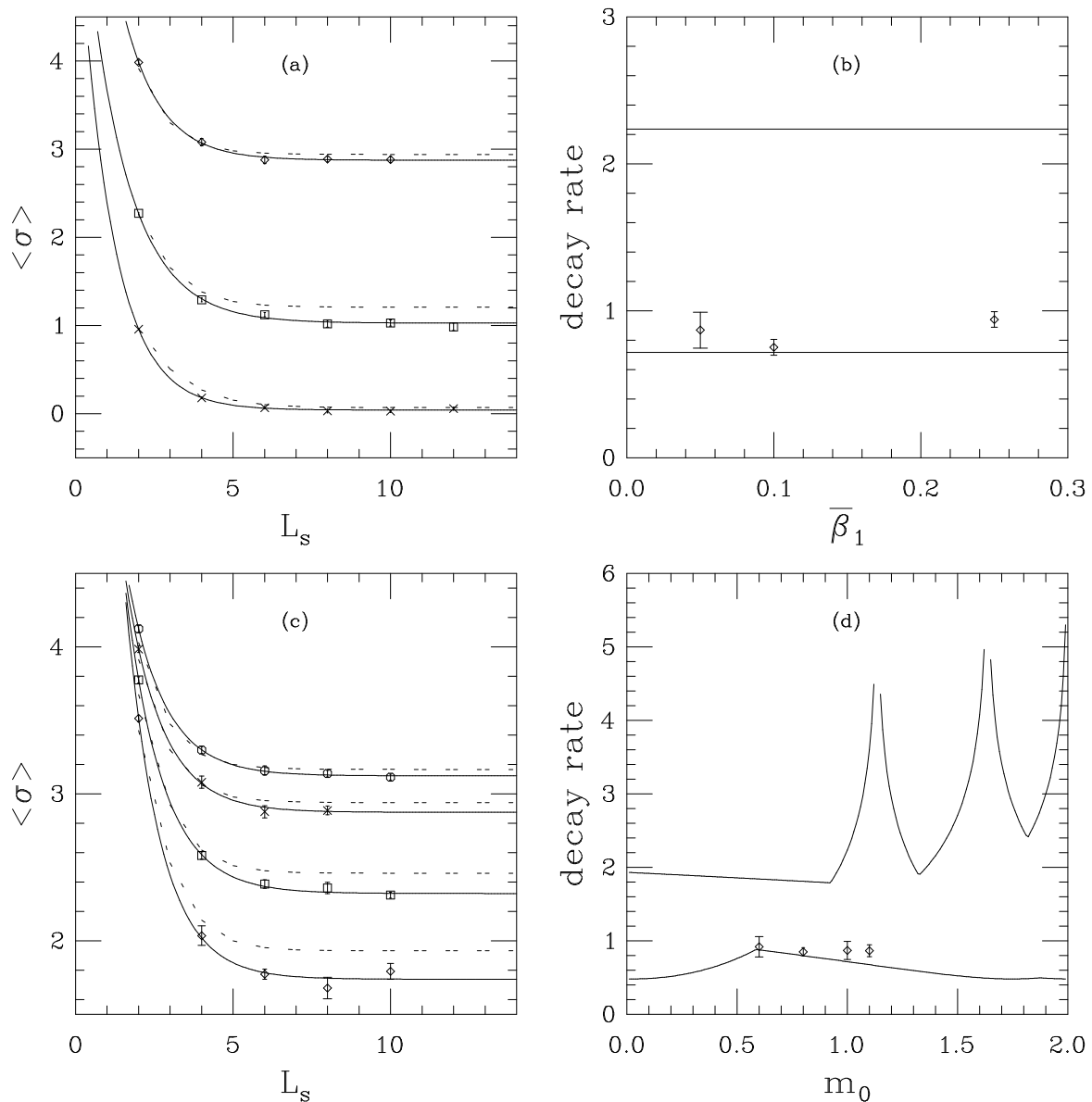


Figure 7. The decay and decay rate of $\langle \sigma \rangle$ as a function of L_s for the $Z_2 \times Z_2$ model on a 6^3 lattice with antiperiodic boundary conditions along the time direction and $m_f = 0.02$. In figure 7a $m_0 = 1.0$ and $\bar{\beta}_1 = 0.05$ (diamonds), $\bar{\beta}_1 = 0.1$ (squares) and $\bar{\beta}_1 = 0.25$ (crosses). In figure 7c $\bar{\beta}_1 = 0.05$ and $m_0 = 0.6$ (diamonds), $m_0 = 0.8$ (squares), $m_0 = 1.0$ (crosses), and $m_0 = 1.1$ (circles). The solid lines in figures 7a and 7c are fits to $c_0 + c_1 e^{-c_2 L_s}$ and the dotted lines are the large N predictions. The decay rates c_2 from the fits in figures 7a and 7c are shown in figures 7b and 7d respectively. The solid lines in these figures are the large N predicted minimum and maximum decay rates.

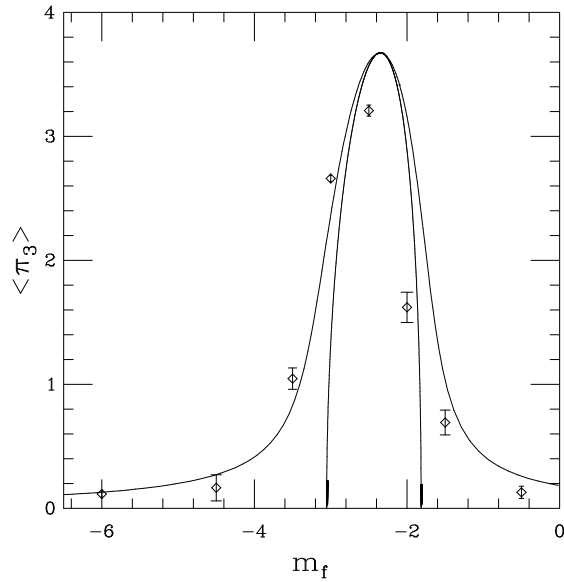


Figure 8. The average value of the third component of the pion field versus m_f for the $SU(2) \times SU(2)$ model on a 6^3 lattice with antiperiodic boundary conditions along the time direction, $\mathbf{h} = (0, 0, 0.1)$, $\bar{\beta}_1 = 0.05$, $L_s = 2$ and $m_0 = 1.0$. The “outer” solid line is the large N prediction for $\mathbf{h} = (0, 0, 0.1)$ and the “inner” one for $\mathbf{h} = (0, 0, 0)$. The diamonds are the results of the numerical simulations.